Kinetic controls on the formation of metastable phases during the experimentally induced breakdown of chlorite

K. A. WALDRON,* G. T. R. DROOP AND P. E. CHAMPNESS

Department of Geology, The University of Manchester, Manchester M13 9PL, U.K.

Abstract

The kinetics and reaction mechanisms of chlorite breakdown have been studied in a series of experiments at conditions similar to those achieved during contact metamorphism (T = 600–725 °C, P = 1 kbar). Cores of chlorite schist were used as starting material in order to simulate natural metamorphic systems and preserve reaction textures. Reaction products were analysed by electron microprobe, scanning- and transmission-electron microscopy (SEM, TEM). Although the texture of the original chlorite was preserved in experiments run below 680 °C, talc had replaced chlorite. Olivine and spinel formed along grain boundaries, indicating long-range diffusion of aluminium. Above 680 °C the chlorite was replaced by patches of disordered, aluminous pyroxene. Olivine and spinel grew both within the pyroxene and along what are believed to be former chlorite grain-boundaries. Reactions relevant to the observed textures and assemblages are:

$$\text{Chl} = \text{Tlc} + \text{Ol} + \text{Spl} + \text{H}_2\text{O}$$
$$\text{Chl} = \text{Opx} + \text{Ol} + \text{Spl} + \text{H}_2\text{O}$$

Thermodynamic calculations show that both of these reactions are metastable in the FeO–MgO–Al_2O_3–SiO_2–H_2O system in the P–T range of our experiments. In addition, previous experimental studies and our calculations indicate that the stable reaction is:

$$\text{Chl} = \text{Crd} + \text{Ol} + \text{Spl} + \text{H}_2\text{O}.$$

The absence of cordierite in the run products, and the formation of talc and orthopyroxene while thermodynamically metastable, show that the ease of nucleation of these phases controlled the reaction mechanisms in the early stages.

KEYWORDS: chlorite breakdown, reaction mechanisms, kinetics, metastable, talc, orthopyroxene, spinel, olivine.

Introduction

IN metamorphic environments where heating and cooling are rapid, chemical and textural equilibrium may not be achieved and mineral transformations may be incomplete. Disequilibrium reaction textures are occasionally preserved in contact metamorphic rocks and record evidence of the stages of mineral transformation. Natural examples of these 'stranded' textures have yielded information about the reaction mechanisms of the thermal decomposition of glaucophane (Wirth, 1986), biotite (Brearley, 1987*a*), muscovite (Brearley, 1986), chlorite and phengite (Worden *et al.*, 1987, 1988, 1992). Some workers have attempted to induce the disequilibrium breakdown of biotite and muscovite and to put temperature–time limits on the formation of these textures by experimentally simulating pyrometamorphic conditions in natural rock cores (Brearley, 1987*b*; Bearley and Rubie, 1990; Rubie and Brearley, 1987, 1991). We have used similar techniques to investigate the kinetics and mechanisms of chlorite breakdown.

Chlorite breakdown was chosen for several reasons. Firstly, chlorite is a common and abundant constituent of low-grade metamorphic rocks and its breakdown is therefore an important part of the reaction history of many metamorphic rocks. Secondly, there have been numerous

* Present address: Department of Geology, Colgate University, Hamilton, NY 13346, USA.

Mineralogical Magazine, March 1993, Vol. 57, pp. 141–156

experimental studies of chlorite stability in the ideal $MgO–Al_2O_3–SiO_2–H_2O$ (MASH) and $FeO–MgO–Al_2O_3–SiO_2–H_2O$ (FMASH) systems (Roy and Roy, 1955; Nelson and Roy, 1958; Fawcett and Yoder, 1966; Velde, 1973; Chernosky, 1974; McOnie *et al.*, 1975; Fleming and Fawcett, 1976; Jenkins and Chernosky, 1986). Thirdly, natural examples of disequilibrium chlorite breakdown from contact aureoles have been described (Worden *et al.*, 1987, 1988). The results of experiments in the ideal systems and observations of natural chlorite breakdown textures provide a good framework for the analysis of experiments in which rock cores are used as starting material. Fourthly, workers who used natural muscovite schists and biotite schists as starting materials (Rubie and Brearley, 1987, 1990; Brearley and Rubie, 1990; Brearley, 1987*b*) have produced disequilibrium reaction textures containing appreciable amounts of reaction products within reasonably short run times (10s to 100s of hours). It was thought that, as another phyllosilicate, chlorite would also break down easily.

Most experimental studies of chlorite stability have been designed to determine the location of equilibria in ideal chemical systems (see above references). The starting materials used in these earlier studies were pure, powdered oxide reagents and/or powdered, synthetic, crystalline phases. The use of pure starting materials allows correlation of experimental results with previous experiments and theoretically derived thermodynamic models. Use of powdered materials ensures rapid reaction rates and allows equilibrium to be established in experimentally reasonable times. In our experiments we used small cores of natural chlorite schist as starting material. Although it was difficult to control fully the homogeneity of the starting material in terms of composition and grain size, we hoped that the use of rock cores rather than powders would simulate natural systems and preserve textural evidence of the processes involved in metamorphism.

Methods

Starting material. The rock used in this study was chosen for its simple assemblage, the abundance and composition of the chlorite and the chlorite's apparent textural and chemical homogeneity. A magnesian chlorite schist was used because of the abundance of experimental data on the stability of Mg end-member chlorite (clinochlore). In order to simplify the experimental system and to minimise the number of possible reactions, a nearly monomineralic chlorite schist was chosen. In a preliminary set of experiments we used a chlorite + quartz schist that contained minor amounts of calcite and albite. It was found that, even at the lowest run temperatures, Ca and Na participated in the chlorite breakdown reactions. Both chlorite + quartz reactions and chlorite decomposition reactions occurred in these runs, making textural and kinetic interpretation very difficult.

The rock used in the present study is from a blackwall zone adjacent to a serpentinite body in lower Kaponig Tal, S.E. Tauern Window, Austria. It is a magnesian chlorite + magnetite schist and consists of pale green, interlocking chlorite laths (>0.50 mm long, 0.01–0.10 mm wide) and large, euhedral, magnetite crystals (1–2 mm diameter). The chlorite has a composition which falls entirely within the $FeO–MgO–Al_2O_3–SiO_2–H_2O$ (FMASH) system, excepting a trace of TiO_2, and has an Mg/(Mg + Fe) value of 0.75–0.79 (Table 2). Small amounts of talc are present around the magnetite crystals. TEM analyses showed that the chlorite was undeformed and apparently unreacted and that there was no evidence of its being intergrown with another phyllosilicate (e.g. talc).

Experimental procedure. Experiments were performed in cold-seal apparatus at the Grant Institute of Geology, Edinburgh University. Cores of starting material were prepared by cutting small rods from the rock and turning them on a diamond lap until smooth cores (12–15 mm long, 3–4 mm diameter, 0.14–0.20 g weight) were produced. Cores were welded into Pt capsules, which were then placed in cold-seal bombs and stabilised at 1 kbar pressure (Ar gas pressure medium) before being heated to the desired run temperature. Temperature and pressure were recorded regularly during the experiments. Temperature could be determined to within ±2 °C and pressure to within ±0.1 kbar. At the end of each run, the experiments were quenched using a pressurised air collar fitted over the bomb. The temperature of the bomb during quenching dropped below 300 °C within five minutes. The cooled capsules were weighed and opened. The cores were extracted and weighted. Doubly-polished thin sections and polished blocks were made from each core. These materials were used for petrographic, microprobe, TEM and back-scattered SEM analyses. Table 1 gives the temperature–pressure–time conditions of the experiments.

The experiments were performed without an added buffer because the oxygen fugacity within the bombs was approximately that of the Ni–NiO buffer. The presence of spinel in the run products

Table 1: Pressure-temperature-time conditions of chlorite breakdown experiments. *poor temperature control during heating (>100°C overstep of desired temperature), #capsule failure. Temperatures have a maximum uncertainty of 5°C.

Experiment	T (°C)	P (kbar)	Duration (hours)
C101*	700	1	168
C102	700	1	335
C103#	660	1	168
C104	642	1	168
C105	640	1	599
C106	601	1	335
C107	660	1	168
C108	725	1	168
C109	721	1	599

Table 2: Representative compositions of chlorite. 898 is the chlorite in our starting material, and W is the composition of regional metamorphic chlorite reported by Worden et al. (1987, Table 2). Other analyses are from the indicated experiments.

	898	W	C104	C105	C107
SiO_2	28.53	24.88	29.30	19.00	28.46
Al_2O_3	20.06	21.01	18.68	19.00	19.62
FeO	14.41	30.66	13.88	13.65	13.96
MgO	25.22	11.28	25.60	24.68	24.39
TiO_2	0.10	0.0	0.10	0.01	0.0
MnO	0.04	0.0	0.16	0.04	0.01
Na_2O	n.a.	n.a.	n.a.	0.17	0.41
total	88.36	88.15	87.72	86.08	86.85
oxygens	14.00	14.00	14.00	14.00	14.00
Si	2.81	2.68	2.90	2.87	2.84
$Al^{(iv)}$	1.19	1.32	1.10	1.13	1.16
$Al^{(vi)}$	1.14	1.36	1.08	1.12	1.15
Fe	1.18	2.77	1.14	1.15	1.16
Mg	3.70	1.82	3.77	3.70	3.64
Ti	0.01	0.0	0.0	0.0	0.0
Mn	0.0	0.0	0.01	0.0	0.0
Na	n.a.	n.a.	n.a.	0.04	0.08
total	10.03	9.95	10.00	10.01	10.03
M/FM	0.76	0.40	0.77	0.76	0.76

confirms that the f_{O_2} was buffered near this value. It was assumed that $P_{total} = P_{H_2O}$ during the experiments because any amount of chlorite breakdown releases water and all capsules emitted a vapour phase when opened at the end of the experiments.

Results

The observations described below were made using optical microscopy, electron microprobe analysis (energy-dispersive analyses with the Cameca Camebax at the University of Manches-

Table 3: Representative compositions of spinel and olivine. Fe^{3+} calculated by the method described by Droop (1987). * indicates $Mg/(Fe^{2+} + Mg)$.

	spl C105	spl C109	spl C108	ol C107	ol C109	ol C108
SiO_2	3.06	3.07	4.91	37.92	38.31	37.39
Al_2O_3	56.14	60.90	60.20	1.22	0.16	0.41
FeO	14.81	17.55	17.97	19.76	20.29	17.38
Fe_2O_3	8.90	--	--	0.00	0.00	0.00
MgO	17.83	17.57	18.73	41.96	40.02	39.88
TiO_2	0.06	n.a.	0.08	0.0	0.04	0.00
MnO	0.04	n.a.	0.15	0.17	0.18	0.16
Na_2O	0.75	n.a.	0.20	n.a.	n.a.	0.09
total	101.59	99.11	102.24	101.03	99.00	95.31
oxygens	32.00	32.00	32.00	4.00	4.00	4.00
Si	0.63	0.64	0.98	0.96	1.00	1.00
Al	13.94	14.85	14.21	0.04	0.01	0.01
Fe^{2+}	2.55	3.04	3.01	0.42	0.44	0.39
Fe^{3+}	1.38	--	--	0.00	0.00	0.00
Mg	5.48	5.42	5.59	1.60	1.55	1.60
Ti	0.01	n.a.	0.01	0.00	0.00	0.00
Mn	0.01	n.a.	0.03	0.00	0.00	0.00
Na	0.30	n.a.	0.08	n.a.	n.a.	0.00
total	24.00	23.95	23.91	3.02	3.00	3.00
M/FM	0.68*	0.64	0.65	0.79	0.78	0.80

ter, operated at 15 kV, and wavelength-dispersive analyses with the Cameca Camebax at the University of Edinburgh, operated at 20 kV) SEM (JEOL JSM-6400 at the University of Manchester) and TEM (Philips EM430 at the University of Manchester/UMIST operating at 300 kV). Back-scattered electron (BSE) images were obtained with the microprobes and the SEM. Mineral analyses are listed in Tables 2–5.

C106 (601 °C, 335 hrs). No changes in the original texture or chemistry were detected.

C104 (642 °C, 168 hrs). Chlorite laths retain their original appearance and grain boundaries are generally smooth and straight. Chlorite–chlorite grain boundaries often contain grains of an opaque phase that are <3 μm in diameter. This phase is also sometimes found along chlorite cleavage planes. The grains are too small for quantitative microprobe analysis, but qualitative analysis shows that they are rich in Fe and Mg and have a high Al content and are therefore probably spinel. Another grain-boundary phase has Si, Mg and Fe concentrations indicative of olivine. The chlorite has its original composition. A few

Table 4: Representative compositions of talc.

	C104	C105	C107
SiO_2	59.26	61.75	61.96
Al_2O_3	1.77	0.03	0.21
FeO	5.64	6.11	6.70
MgO	27.16	26.82	26.95
TiO_2	0.06	0.08	0.02
MnO	0.02	0.02	0.05
Na_2O	n.a	0.06	0.26
total	93.91	94.87	96.15
oxygens	22.00	22.00	22.00
Si	7.81	8.05	8.00
Al	0.28	0.0	0.04
Fe	0.62	0.67	0.72
Mg	5.34	5.21	5.19
Ti	0.01	0.01	0.0
Mn	0.0	0.0	0.0
Na	n.a.	0.02	0.01
total	14.06	13.97	13.96
M/FM	0.90	0.89	0.88

Table 5: Representative compositions of pyroxene.

	C102	C102	C108
SiO_2	53.70	50.10	51.52
Al_2O_3	8.43	11.70	10.30
FeO	5.60	6.66	6.37
MgO	23.45	22.73	22.62
TiO_2	0.21	0.10	0.15
MnO	0.04	0.02	0.05
Na_2O	n.a.	n.a.	0.23
total	91.43	91.31	91.24
oxygens	6.00	6.00	6.00
Si	1.98	1.87	1.92
$Al^{(iv)}$	0.02	0.13	0.08
$Al^{(vi)}$	0.35	0.39	0.37
Fe	0.17	0.21	0.20
Mg	1.29	1.26	1.26
Ti	0.01	0.0	0.0
Mn	0.0	0.0	0.0
Na	n.a.	n.a.	0.02
total	3.82	3.86	3.85
M/FM	0.88	0.86	0.86

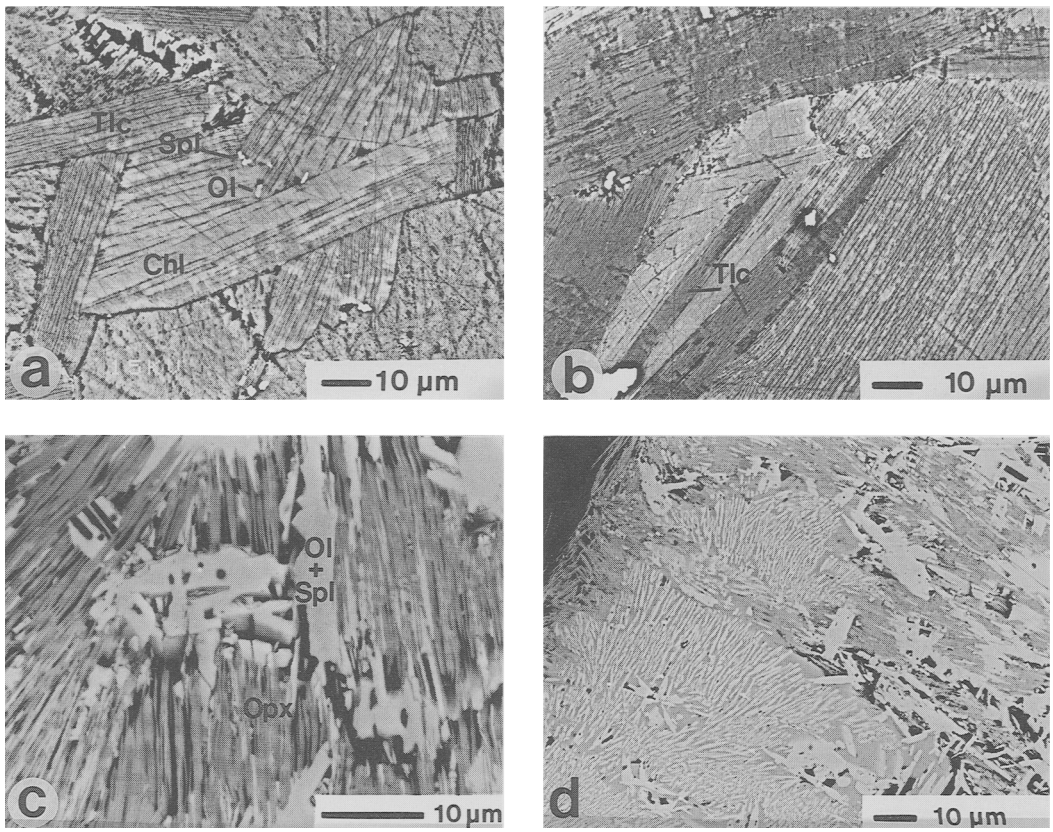

FIG. 1. (*a*) Back-scattered electron (BSE) micrograph of C105 (640 °C, 1 kbar, 599 hours). Chlorite laths (Chl, light grey) have been partially replaced by talc (Tlc, darker material, see discussion in text). The direct replacement of chlorite by talc is facilitated by the similarity between talc and the 'talc' interlayers in the chlorite crystal structure. Bright spots along chlorite grain boundaries are spinel and olivine (Spl, Ol, centre). (*b*) BSE micrograph of C107 (660 °C, 1 kbar, 168 hours). Some chlorite laths have been completely replaced by talc (Tlc, dark laths), but retain the original chlorite texture. Spinel and olivine (bright spots) occur along grain boundaries and selected chlorite cleavage planes. (*c*) BSE micrograph of C109 (721 °C, 1 kbar, 599 hours). Patches of fibrous orthopyroxene (Opx, dark grey) are surrounded by blocky areas comprising intergrowths of olivine (Ol) and spinel (Spl). Olivine and spinel are also finely intergrown with the pyroxene (bright streaks). The fibrous pyroxene–olivine–spinel patches mimic the size and shape of the original chlorite laths. (*d*) BSE micrograph of C102 (700 °C, 1 kbar, 335 hours). Fine intergrowths of pyroxene (dark grey) and olivine and spinel (light grey) are found near the edges of the reacted rock core. This symplectite texture may form when melt produced during the experiment is quenched. This texture was found in all experiments run at or above 700 °C.

chlorite laths have internal bands of talc which appear to have grown along the length of the laths parallel to chlorite cleavage planes. Where developed, the talc may replace more than 50% of the original lath.

C105 (640 °C, 599 hrs). Almost all chlorite laths have been replaced to some extent by talc, spinel and olivine (Fig. 1*a*). Grain-boundary spinel may be up to 10 μm in diameter.

C107 (660 °C, 168 hrs). As in C104 and C105, chlorite laths retain their original texture. While microprobe analysis reveals that a few laths have been completely replaced by talc, most are unreacted chlorite (Fig. 1*b*). Apart from having slightly different BSE intensities, talc and chlorite are texturally indistinguishable. Small grains of spinel and olivine occur along grain boundaries and cleavage planes.

C102 (700 °C, 335 hrs), C108 (725 °C, 168 hrs), C109 (721 °C, 599 hrs). These samples have developed very different textures from those run at lower temperatures. The original chlorite lath texture has been lost and is replaced by spinel, olivine and fibrous, aluminous pyroxene

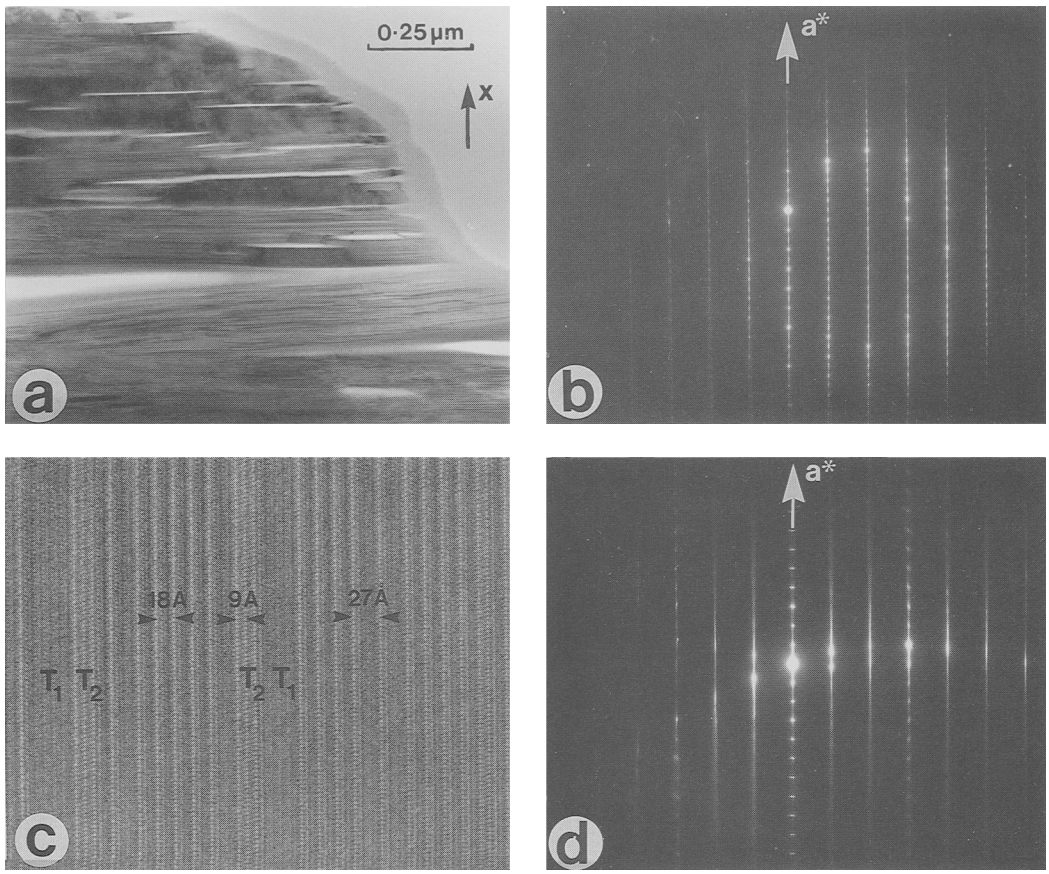

FIG. 2. The microstructure of the pyroxene. (*a*) Electron micrograph showing that the pyroxene consists of bundles of sub-parallel 'fibres' elongated parallel to the (100) plane. Specimen C102 (700 °C, 1 kbar, 335 hours). (*b*) Typical electron diffraction pattern from a pyroxene crystal. The pattern can be indexed as [011] of orthopyroxene. Notice that sharp (9 Å) and diffuse (18 Å) spots alternate parallel to **a*** and are joined by continuous streaks. Specimen C109 (721 °C, 1 kbar, 599 hours). (*c*) High-resolution micrograph of a region that gave the diffraction pattern in (*b*). Notice the variation in the (100) lattice spacing. Twin-related clinopyroxene (9 Å) regions are labelled T_1 and T_2. (*d*) [011] electron diffraction pattern from the region shown in (*a*). The stacking of the (100) layers is so disordered that only 9 Å spots are present. Notice that reciprocal lattice rows for which $k + l \neq 3n$ show continuous streaking parallel to **a*** and only poorly-defined reflections.

(Fig. 1*c*). TEM shows that the pyroxene occurs as sub-parallel fibres approximately 0.7 μm wide which are elongated parallel to their (100) planes (Fig. 2*a*). Electron diffraction indicates that there is considerable stacking disorder of the (100) layers of the pyroxene. Fig. 2*b* can be indexed as an orthopyroxene, but sharp (9 Å) and diffuse (18 Å) spots alternate parallel to **a*** and are joined by continuous streaks. High-resolution images (Fig. 2*c*) confirm that the structure of regions giving such a diffraction pattern is made up of random intergrowths of 9 and 18 Å phases, with occasional 27 Å layers. Some pyroxene grains are even more disordered. Fig. 2*d* is a diffraction pattern from another pyroxene fibre taken in the same orientation as Fig. 2*b*, but in this case there are no 18 Å spots and reciprocal lattice rows for which $k + l \neq 3n$ show continuous streaking parallel to **a*** and only poorly-defined reflections. The pattern indicates that there is 'semi-random stacking' (in the nomenclature of Brown and Bailey, 1962) of the (100) pyroxene oxygen layers with a fault vector equal to $\pm\mathbf{b}/3$. **b** is one of the directions in pyroxene in which the oxygen sub-lattice is approximately close-packed and **b**/3 is approximately equal to the spacing between adjacent oxygen ions. This kind of stacking is common in phyllosilicates such as

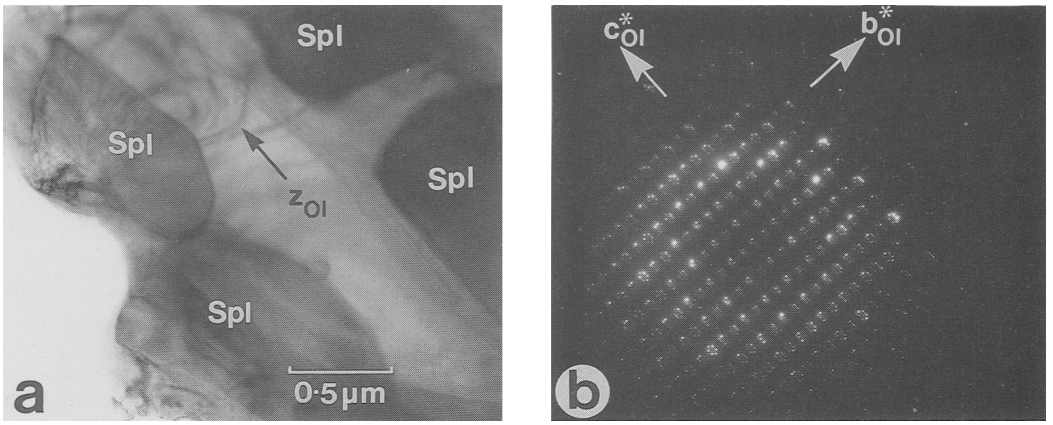

FIG. 3. (*a*) Electron micrograph of olivine and enclosed spinel grains (Spl) from a region of pyroxene fibres in sample C109 (721 °C, 1 kbar, 599 hours). (*b*) Diffraction pattern of the intergrown olivine and spinel in (*a*). The clusters of spots arise by double diffraction between the phases.

chlorite (Brown and Bailey, 1962) and biotite (Bell and Wilson, 1986).

Patches of olivine occur within the regions of fibrous pyroxene and, in turn, spinel grains (up to 1 μm in size) occur within the olivine (Fig. 3*a*). The spinel and olivine are crystallographically oriented with respect to one another (Fig. 3*b*) with:

$$(100)_{Ol}//\{111\}_{Spl};\ [001]_{Ol}//\langle 110\rangle_{Spl}.$$

This is the same orientation relationship as found previously between olivine and magnetite (e.g. Champness, 1970) and corresponds to the closest-packed planes and closest-packed directions being parallel in the two phases.

The composition of the pyroxene was difficult to determine by electron microprobe analysis. The poor wt.% and cation totals (reported in Table 5) are probably the result of the fibrous nature of the phase and its intergrowth with spinel and olivine on a very fine scale. The pyroxene has a rather high and variable Al-content, although similar Al-contents were reported by Worden *et al.* (1987, Table 10) for orthopyroxene from the breakdown of natural chlorite in a metamorphic aureole. The fibrous pyroxene–olivine–spinel intergrowths form patches that tend to mimic the size and shape of the original chlorite laths. On the edges of the fibrous patches (presumably along what were the original chlorite grain boundaries) are coarse (up to 10 × 50 μm), somewhat blocky areas which comprise complex intergrowths of spinel and olivine. Individual crystals of spinel and olivine were not resolved using BSE, but elemental X-ray maps and microprobe analyses from the same blocky area (Table 3) confirm that the two minerals are finely intergrown in approximately equal modal proportions. Talc was not detected in these experiments, but in samples run for 335 hrs at 700 °C and for 168 hrs at 725 °C, rare, remnant chlorite occurs as irregular, ragged areas bordering the pyroxene. The absence of talc and presence of remnant chlorite suggest that pyroxene may have replaced chlorite directly, rather than having been preceded by talc formation. Fine intergrowths of pyroxene and olivine crystals are found near the edges of the rock core (Fig. 1*d*). These resemble quench textures and may indicate the presence of a melt phase during the experiment.

The textural features observed can be summarised as follows:

(*a*) Between 640–660 °C chlorite is partially replaced by talc. In experiments of short duration (168 hours) only a few chlorite laths show evidence of replacement, while most laths in the longer experiment (599 hours) were partially replaced. In either case, the original lath texture is retained. Spinel and olivine are found along grain boundaries and, to a lesser extent, along (001) chlorite cleavage-planes.

(*b*) At 700 °C and above chlorite is replaced by aluminous pyroxene, spinel and olivine. The original lath texture is lost, although fibrous orthopyroxene–spinel–olivine intergrowths mimic the lath shapes. Olivine and spinel also occur in complex intergrowths along the original chlorite grain boundaries.

Interpretation

Stable equilibrium phase relations. Interpretation of our experimental results requires com-

parison with data on stable equilibrium phase relations. In the pure $MgO–Al_2O_3–SiO_2–H_2O$ (MASH) system, the four most likely terminal chlorite-breakdown reactions are:

$$MgChl = MgOpx + Fo + MgSpl + H_2O \quad (1)$$

$$MgChl = MgAth + Fo + MgSpl + H_2O \quad (2)$$

$$MgChl = Fo + MgCrd + MgSpl + H_2O \quad (3)$$

$$MgChl = Fo + MgTlc + MgSpl + H_2O, \quad (4)$$

(see Appendix for abbreviations of mineral names). Information on the relative stabilities of equilibria 1–4 has been gained from experimental studies and thermodynamic calculations. The experimental studies (Roy and Roy, 1955; Nelson and Roy, 1958; Fawcett and Yoder, 1966; Velde, 1973; Chernosky, 1974; Fleming and Fawcett, 1976; Jenkins and Chernosky, 1986) show that between 1 and 3 kbar, and in the temperature range of interest, reaction 3 is the stable terminal reaction in the MASH system. According to Fawcett and Yoder (1966), Chernosky (1974) and Jenkins and Chernosky (1986), reaction 1 becomes stable relative to reaction 3 at pressures above 3 kbar and temperatures above 750–800 °C and the equilibrium assemblage becomes En + Fo + Spl. This means that, in the MASH system, enstatite is stable above 3 kbar and cordierite is stable below 3 kbar.

We came to similar conclusions from thermodynamic calculations. Equilibria among the components clinochlore, amesite, talc, Mg-Tschermaks talc, enstatite, Mg-Tschermaks pyroxene, forsterite, Mg–spinel, Mg–cordierite, corundum, chrysotile, β-quartz and aqueous fluid were calculated for the MASH system at 1 kbar and unit water activity using the program THERMOCALC (Powell and Holland, 1988) in conjunction with the self-consistent thermodynamic dataset of Holland and Powell (1990) and the activity models listed in Table 6. Equilibria involving aluminous orthoamphibole could not be calculated owing to the absence of thermodynamic data for an aluminous anthophyllite component in the dataset used.

The results of the 1 kbar MASH calculations are presented in Table 7 and Fig. 4; the key points are as follows:

(*a*) At 1 kbar, the most thermally stable Mg-chlorite has a composition close to $Clin_{75}Ames_{25}$ and breaks down to Fo + MgCrd + MgSpl by rection 3 at ~664 °C.

(*b*) Reactions 1 and 4 are both metastable with respect to reaction 3. However, the temperature differences (~4 °C between 1 and 3, ~6 °C between 4 and 3) are small and similar in size to the 1σ error on the equilibrium temperature of each reaction.

(*c*) Mg-chlorites with compositions between $Clin_{75}Ames_{25}$ and $Clin_{85}Ames_{15}$ begin to break down at a temperature between ~655 °C and 664 °C (depending on composition) to forsterite, Mg-cordierite and more aluminous Mg-chlorite by the continuous reaction

$$MgChl = MgCrd + Fo + Al_2Mg_{-1}Si_{-1} + H_2O, \quad (5)$$

which proceeds with rising temperature until reaction 3 is intersected.

(*d*) Mg-chlorites with compositions less aluminous than $Clin_{85}Ames_{15}$ begin to break down at a temperature below ~655 °C to forsterite, more aluminous Mg-chlorite and aluminous Mg-talc by the continuous reaction

$$MgChl = Fo + MgTlc + Al_2Mg_{-1}Si_{-1} + H_2O, \quad (6)$$

which continues until ~655 °C at which point the discontinuous reaction

$$MgChl + MgTlc = Fo + MgCrd + H_2O \quad (7)$$

occurs. Further Mg-chlorite decomposition then takes place by reactions 5 and 3. In the MASH system, therefore, talc appears as a stable intermediate breakdown product of low-alumina Mg-chlorite.

(*e*) Orthopyroxene is not a stable breakdown product of any Mg-chlorite composition, though it does appear as a stable phase in bulk compositions less aluminous than the forsterite-Mg-cordierite joint at temperatures above ~649 °C.

(*f*) Corundum is a stable intermediate breakdown product of Mg-chlorites with compositions more aluminous than $Clin_{53}Ames_{47}$.

Adding iron to the system will make equilibria 1–4 divariant (univariant at constant pressure), and should allow chlorite to coexist with four dehydration product phases (three solid, one fluid) over a finite temperature interval. The experiments of McOnie *et al.* (1975) in the $FeO–MgO–Al_2O_3–SiO_2–H_2O$ (FMASH) system at 2.07 kbar lead to the following conclusions regarding reaction 3; (*a*) the reaction is stable for the chlorite composition range Mg/(Mg + Fe) = 0.5–1.0, (*b*) it must have a very narrow divariant field (<20 °C), and (*c*) the equilibrium temperature decreases slightly as Mg/(Mg + Fe) decreases [60 °C lower for Mg/(Mg + Fe) = 0.5 compared with 1.0]. Neither talc nor orthopyroxene appeared as a stable breakdown product in McOnie *et al.* (1975), but both appeared as metastable products which disappeared with increased time.

Table 6: Activity models used in calculations. See Appendix for component abbreviations.

Component	Formula	Activity Model	
Clin	$Mg_4^{M1}Mg^{M2}Al^{M2}Al^{T2}Si^{T2}Si_2^{T1}O_{10}(OH)_8$	$16(X_{Mg}^{M1})^4.(X_{Mg}^{M2}).(X_{Al}^{M2}).(X_{Al}^{T2}).(X_{Si}^{T2})$	.....(1)
Ames	$Mg_4^{M1}Al_2^{M2}Al_2^{T2}Si_2^{T1}O_{10}(OH)_8$	$(X_{Mg}^{M1})^4.(X_{Al}^{M2})^2.(X_{Al}^{T2})^2$	.....(1)
MgCrd	$Mg_2Al_4Si_5O_{18}$	$(X_{Mg})^2$	.....(3)
Fo	Mg_2SiO_4	$(X_{Mg})^2$	.....(3)
MgSpl	$MgAl_2O_4$	$(X_{Mg}).(X_{Al})^2$	.....(3)
MgTa	$Mg_2^{M1}Mg^{M2}Si_2^{T2}Si_2^{T1}O_{10}(OH)_2$	$(X_{Mg}^{M1})^2.(X_{Mg}^{M2}).(X_{Si}^{T2})^2$	.....(1)
TaTs	$Mg_2^{M1}Al^{M2}Al^{T2}Si^{T2}Si_2^{T1}O_{10}(OH)_2$	$4(X_{Mg}^{M1})^2.(X_{Al}^{M2}).(X_{Al}^{T2}).(X_{Si}^{T2})$	.....(1)
En	$Mg^{M2}Mg^{M1}Si_2^TO_6$	$(X_{Mg}^{M2}).(X_{Mg}^{M1})$	.....(2)
MgTs	$Mg^{M2}Al^{M1}Al^TSi^TO_6$	$(X_{Mg}^{M2}).(X_{Al}^{M1})$	.....(2)

Sources: (1): Holland and Powell (1990); (2): Wood and Banno (1973); (3): Assumes ideal ionic mixing.

The foregoing conclusions are supported in all important respects by our thermodynamic calculations. THERMOCALC results for the FMASH system indicate that Mg/(Mg + Fe) values of coexisting minerals increase in the order Spl ≪ Ol ≪ Opx ≪ Chl < Tlc ≈ Crd at any given temperature in the range 600–660 °C. The effect of this is to lower the equilibrium temperatures of reactions 1, 3 and 4 with increasing iron content (Fig. 5). The decreases in temperature of 3 and 4 for a given increase in the iron content of chlorite are similar to one another and larger than the temperature decrease of 1, with the result that 3 is the stable FMASH isobaric univariant chlorite breakdown reaction at 1 kbar over a wide range of chlorite Mg/(Mg + Fe) values (Fig. 5).

Another implication of the calculated Fe/Mg partitioning data is that the equilibrium curve of the reaction

$$\text{Fo} + \text{MgCrd} = \text{MgOpx} + \text{MgSpl}, \quad (8)$$

which has a low dP/dT and occurs at $P > 2.5$ kbar in the MASH system (see also Fawcett and Yoder, 1966; Seifert, 1974; Herzberg, 1983), is deflected to higher pressures with increasing iron content, consistent with reaction 1 becoming progressively more metastable at 1 kbar.

The calculated alumina content of chlorite coexisting with olivine, cordierite, spinel and H_2O increases with increasing iron content from ~25% Ames at Mg/(Mg + Fe) = 1.0 through ~33% Ames at Mg/(Mg + Fe) = 0.69.

The calculated sequences of stable equilibrium breakdown reactions of low-alumina chlorites in the FMASH system mimic those in the iron-free system. As in the MASH system, talc can only appear as a stable product if the alumina content of the original chlorite is low enough (Ames + Fe-

Table 7. Isobaric invariant equilibria among the phases chlorite, talc, orthopyroxene, olivine, cordierite, spinel, corundum, chrysotile and quartz in the MgO-Al_2O_3-SiO_2-H_2O system at 1.0 kbar and unit water activity, calculated using the thermodynamic data of Holland and Powell (1990) and the activity models in Table 6. One-sigma errors on individual temperatures are typically in the range 3-6°C. The quantities X^{Chl}_{Ames}, X^{Tlc}_{TaTs} and X^{Opx}_{MgTs} are measures of the Tschermak contents of chlorite, talc and orthopyroxene, respectively; $X^{Chl}_{Ames} = 2(X^{M2}_{Al}-1) = 2(X^{T2}_{Al}-1)$; $X^{Tlc}_{TaTs} = X^{M2}_{Al} = 2X^{T2}_{Al}$; $X^{Opx}_{MgTs} = X^{M1}_{Al} = 2X^{T}_{Al}$. Numbered equilibria are mentioned in the text. All listed equilibria are stable apart from chlorite terminal equilibria 1 and 4. See appendix for abbreviations.

T (°C)	Equilibrium	X^{Chl}_{Ames}	X^{Tlc}_{TaTs}	X^{Opx}_{MgTs}
707	MgTa = En + Qtz + H_2O	-	0.00	0.00
670	(4) MgChl = MgTlc + Fo + MgSpl + H_2O	0.25	0.16	-
668	(1) MgChl = MgOpx + Fo + MgSpl + H_2O	0.25	-	0.05
665	Fo + MgTlc = MgOpx + MgCrd + H_2O	-	0.12	0.03
664	(3) MgChl = Fo + MgCrd + MgSpl + H_2O	0.25	-	-
655	(7) MgChl + MgTlc = Fo + MgCrd + H_2O	0.15	0.13	-
649	Fo + MgTa = En + H_2O	-	0.00	0.00
621	MgChl + Crn = MgCrd + MgSpl + H_2O	0.47	-	-
427	Chr = Fo + MgTa + H_2O	-	0.00	-

Ames < 15%). On heating, slightly more aluminous chlorites should undergo the FMASH equivalent of reaction 5,

$$\text{Chl} = \text{Ol} + \text{Crd} + \text{MgFe}_{-1} + \text{Al}_2\text{Mg}_{-1}\text{Si}_{-1} + \text{H}_2\text{O}, \quad (9)$$

before intersecting the continuous reaction

$$\text{Chl} = \text{Ol} + \text{Crd} + \text{Spl} + \text{MgFe}_{-1} + \text{MgSiAl}_{-2} + \text{H}_2\text{O}. \quad (10)$$

This is the FMASH equivalent of reaction 3 and proceeds with rising temperature and increasing Mg/(Mg + Fe) values of all minerals (Fig. 5) until the olivine–cordierite–spinel plane intersects the bulk composition of the precursor chlorite, at which point chlorite should finally disappear.

Table 8 summarises the results of our equilibrium calculations on the decomposition path of the chlorite used in our experiments (898 in Table 2). At 1 kbar and unit water activity, chlorite of this composition should break down to combinations of cordierite, olivine, and spinel over a 40 °C temperature interval (~600–640 °C). Neither talc nor orthopyroxene nor corundum should appear as stable phases (though talc is almost stable at ~600 °C). The final chlorite should have an Mg/(Mg + Fe) value of ~0.92.

Comparing the run temperatures of our experiments with Table 8, we conclude that while little or no reaction should have occurred in the 601 °C run (C106), the stable mineral assemblage in all the other runs (>640 °C) should have been Crd + Ol + Spl.

Observed reactions. The reactions that actually occurred in our experiments are:

$$\text{Chl} = \text{Tlc} + \text{Ol} + \text{Spl} + \text{H}_2\text{O} \quad (11)$$

$$\text{Chl} = \text{Opx} + \text{Ol} + \text{Spl} + \text{H}_2\text{O} \quad (12)$$

These reactions are equivalent to reactions 4 and 1, respectively, and are metastable in the FMASH system.

It is inevitable that chlorite breakdown

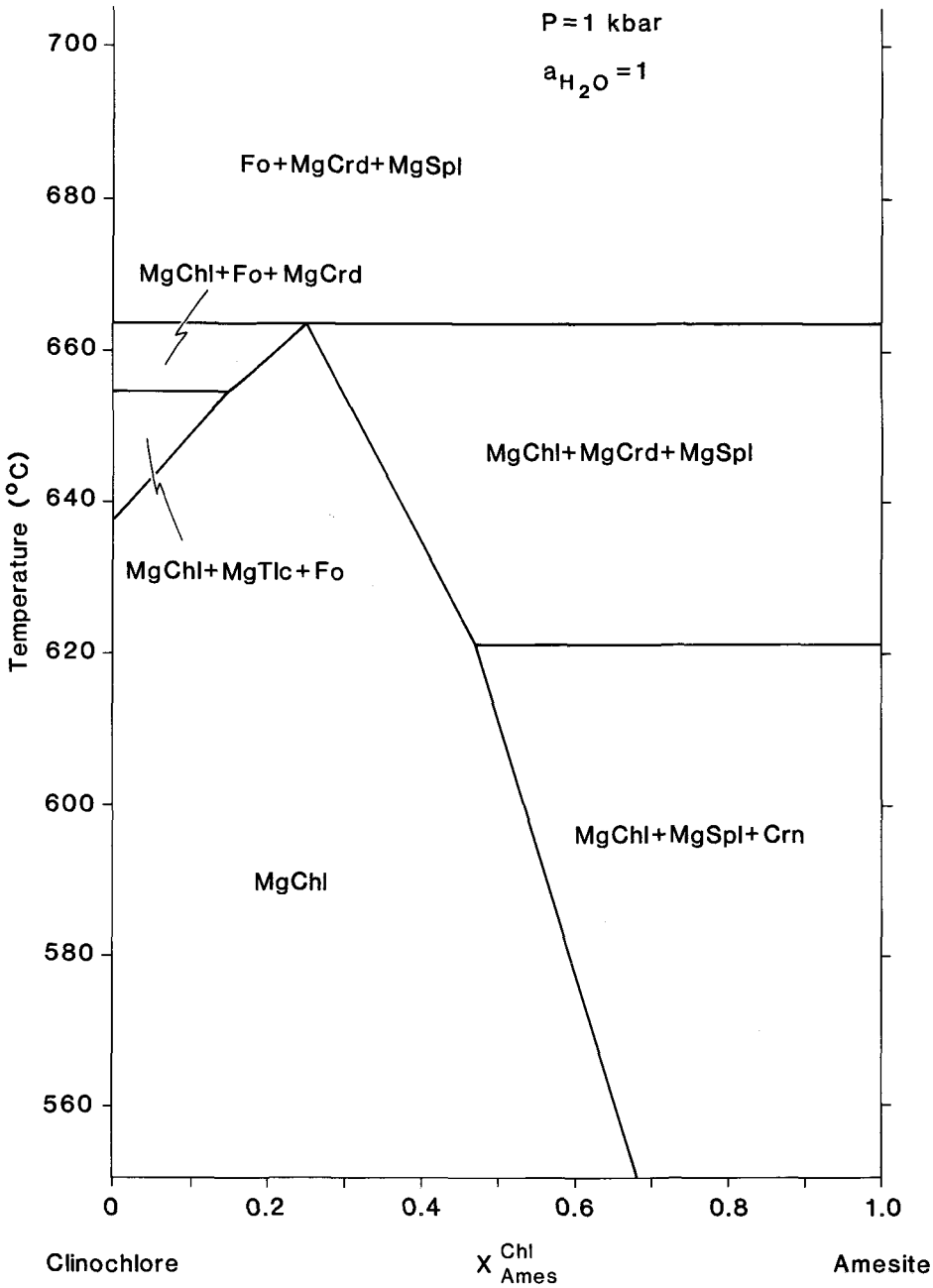

FIG. 4. The clinochlore-amesite pseudobinary section in the $MgO–Al_2O_3–SiO_2–H_2O$ system calculated for 1 kbar pressure and unit water activity using the thermodynamic data of Holland and Powell (1990) and activity models in Table 6. See Appendix for abbreviations of mineral names.

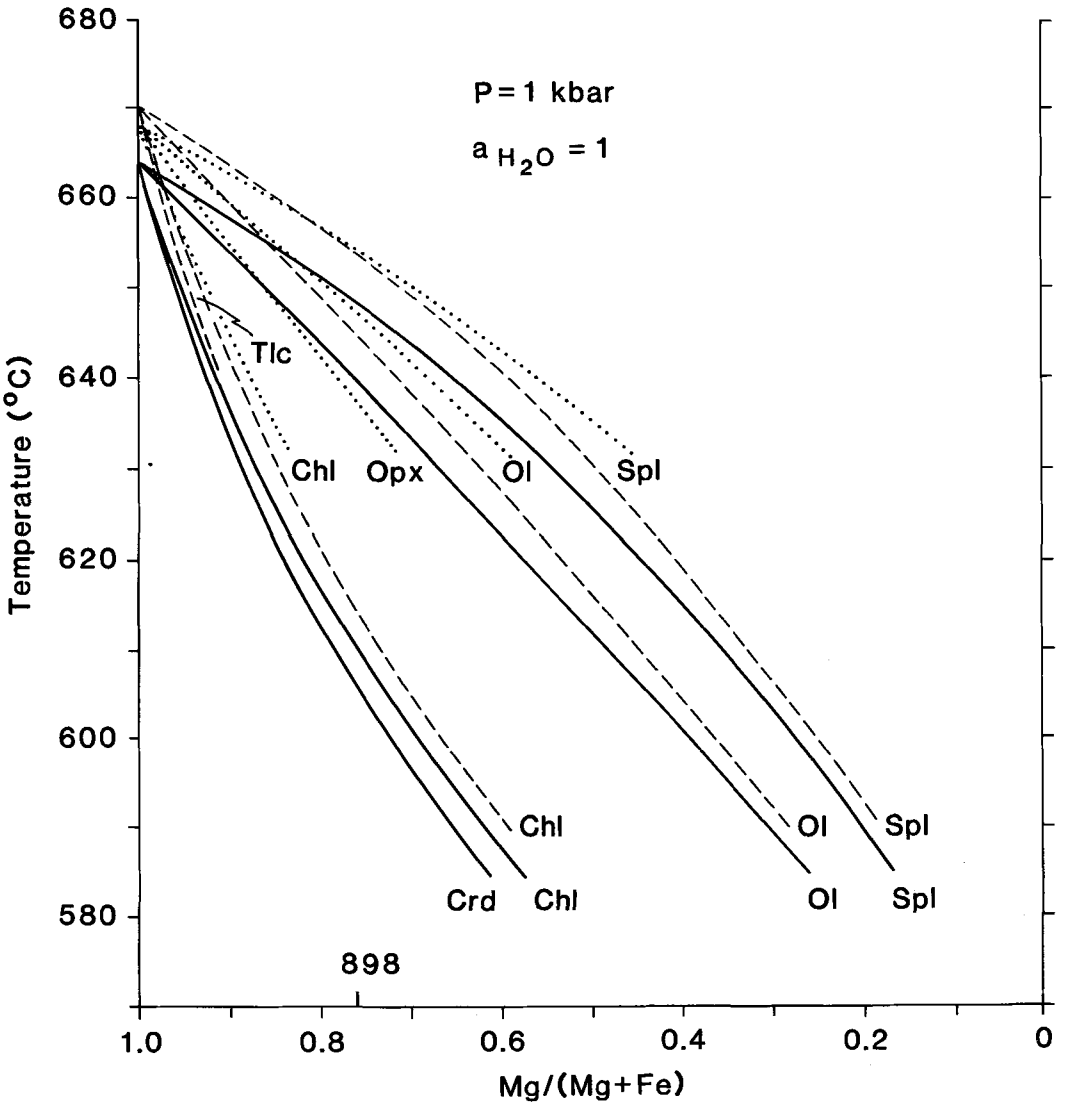

FIG. 5. *T–X*(Mg,Fe) plot showing how Mg/(Mg + Fe) values of coexisting minerals vary with temperature in the assemblage chlorite + cordierite + olivine + spinel + H_2O (solid lines), the assemblage chlorite + talc + olivine + spinel + H_2O (dashed lines) and the assemblage chlorite + orthopyroxene + olivine + spinel + H_2O (dotted lines). Calculated using the thermodynamic data of Holland and Powell (1990). Note that the talc- and orthopyroxene-bearing assemblages are metastable with respect to the cordierite-bearing one. 898 is the composition of the precursor chlorite.

occurred by disequilibrium processes. In none of the experiments was the precursor chlorite heated slowly through the 600–640 °C temperature interval, and in no instance, therefore, did it have the opportunity to undergo reactions 9 and 10 under equilibrium conditions. Consistent with the non-attainment of equilibrium is the fact that chlorite is present in the products of experiment C107, run at 660 °C. This temperature is ~20 °C higher than that at which we predict all chlorite should have disappeared, and ~60 °C higher than that at which the original chlorite composition becomes metastable (Table 8). Also consistent is the observation that the chlorites in the ~640 °C runs

Table 8. Temperature ranges of stable equilibrium mineral assemblages in a bulk composition $Mg_{3.67}Fe_{1.16}Al_{2.34}Si_{2.83}O_{10}(OH)_8$ (a stoichiometric FMASH analogue of the chlorite starting material used in our experiments), calculated for a pressure of 1 kbar and unit water activity using the thermodynamic data of Holland and Powell (1990) and the activity models in Table 6. Also shown are the calculated equilibrium compositions of minerals at 'transition' temperatures (temperatures at which the assemblages change). At temperatures above 598°C, compositional parameters for each mineral change smoothly between one 'transition' temperature and the next.

T (°C)	Stable Assemblage	Mg/(Mg+Fe)				% Ames
		Chl	Ol	Crd	Spl	
>640	Ol + Crd + Spl					
640		0.92	0.76	0.93	0.65	26
615 - 640	Chl + Ol + Crd + Spl					
615		0.79	0.52	0.81	0.40	29
598 - 615	Chl + Ol + Crd					
598		0.76	0.47	0.79	-	17
<598	Chl (starting material)	0.76	-	-	-	17

(C104 and C105) show no evidence of significant compositional change during the experiments, of the kind that would be expected [increasing alumina and Mg/(Mg + Fe)] had the chlorites made any chemical adjustment towards the 640 °C terminal equilibrium composition (Table 8). There is, however, evidence for a close approach to Fe/Mg-exchange equilibrium among the anhydrous reaction products, particularly olivine and spinel. Given that the calculated equilibrium constant for olivine–spinel Fe/Mg exchange is virtually independent of temperature in the range 600–730 °C, measured Mg/(Mg + Fe) compositions of coexisting olivine and spinel from run C109 (Table 3) are remarkably close to the predicted values (Table 8).

The orthopyroxene in our experiments exhibits considerable stacking disorder, is variable in composition and has a high Al-content (~18–26% Tschermak components) compared to the calculated composition of orthopyroxene in equilibrium with olivine + spinel in the 700–720 °C range (~6–7% Tschermak components). These features may be a result of the pyroxene growing metastably. Similar compositional and structural variation has been found in metastable phases produced in other disequilibrium reaction experiments (Brearley, 1987*b*).

If chlorite breakdown proceeded via reaction 4 in the 640–660 °C experiments, we would expect to see significant amounts of olivine and spinel in the run products. The expected volume proportion of olivine + spinel : talc would be 1.9 : 1 for pure spinel and forsterite (molar volume data from Robie *et al.*, 1978). This ratio would be even greater for Fe-bearing olivine and spinel. Fig. 1*a* and *b* do not seem to show enough spinel and olivine to balance the apparent amount of talc present. The BSE images may give a false impression of the amount of chlorite that has been converted to talc. In general, darker areas of the chlorite laths have talc composition, but it may be that the poor quality of the sample polish makes some unreacted chlorite appear dark and leads to an overestimate of the amount of talc present. Similarly, olivine and spinel would not be obvious in poorly polished areas, and this would cause an underestimate of the amount of these phases present. The amount of olivine and spinel evident in the BSE images therefore roughly reflects the minimum amount of reaction that has occurred. It seems clear, however, that chlorite breakdown has produced talc + olivine + spinel since no other product phases (such as cordierite, orthopyroxene, or orthoamphibole) have been identified in the 640–660 °C experiments, and olivine and spinel were not present in the starting material.

The absence of cordierite in our run products is unexpected. In the pure MASH system, Cho and Fawcett (1986) synthesised cordierite in one week (168 hrs) at 720 °C and in two weeks (336 hrs) at 710 °C. McOnie *et al.* (1975) found cordierite in FMASH experiments run at 690 °C for 568 hours,

with conditions very similar to those of some of our experiments (C109). Perhaps the most significant difference between our experiments and those of other workers is that the latter used oxide powders as starting materials while we used natural rock cores. The absence of cordierite as a reaction product in our experiments is probably due to the difficulty of nucleating it in a bulk sample of natural rock. In their TEM study of pyrometamorphosed schists Worden *et al.* (1987) found aluminous orthopyroxene and hercynitic spinel as breakdown products of chlorite, but cordierite only occurred near the margins of grains where the reaction was most advanced. Talc and olivine were not found. Worden *et al.* (1987) ascribed the complete absence of olivine and the absence of cordierite in the cores of their chlorites to the effect of the high Fe[Mg/(Mg + Fe) ≈ 0.3] of their chlorite (Table 2), arguing that the assemblage Spl + Opx is stable at much lower pressures in high-Fe pelites than in the pure MASH system. However, our calculations (see above) suggest that this explanation is wrong. Moreover, this argument cannot explain the absence of cordierite in our runs that did not produce orthopyroxene. As the stable phases olivine and spinel have managed to nucleate, nucleation of stable cordierite was, in effect, competing with nucleation of metastable talc below 680 °C and of metastable orthopyroxene at 700 °C and above. The absence of cordierite must therefore be the result of the relative ease of nucleation of talc (or orthopyroxene) compared with that of cordierite. In a study similar to ours involving disequilibrium breakdown of biotite, Brearley (1987*a*) found that spinel nucleated easily in the early stages of his experiments. If both talc (or orthopyroxene at higher T) and spinel nucleate easily, the formation of cordierite would be greatly suppressed.

The structures of chlorite and talc are very similar; chlorite actually contains 'talc layers' parallel to (001). From the textures observed in BSE images, the (001) plane of talc appears to be parallel to the (001) plane of chlorite, as would be expected. Although cordierite also contains six-fold rings of (Si,Al)–O tetrahedra parallel to (001), the rings do not form continuous sheets as they do in chlorite, so there is no long-range resemblance of the two structures. Thus ΔG^*, the activation energy for nucleation, will be very much lower for the nucleation of talc in chlorite than for the nucleation of cordierite. The difficulty of nucleating cordierite in layered silicate structures is illustrated by the fact that it was found to be unoriented in natural chlorite (Worden *et al.*, 1987) and phengite (Worden *et al.*, 1992). It therefore probably nucleated incoherently, consistent with a high value of ΔG^*.

In contrast to cordierite, the other stable phases olivine and spinel both have layers of approximately close-packed oxygen ions (parallel to (100) and {111} respectively). They would be expected to nucleate with their close-packed planes parallel to (001) of chlorite, though no electron diffraction studies have been carried out as yet to confirm this. We have found, in the 700–725 °C experiments, that the close-packed planes and close-packed directions of olivine and spinel (in olivine–spinel intergrowths within pyroxene) are parallel. Worden *et al.* (1988) determined the orientation relationships of reaction products in pyrometamorphosed chlorite to be:

$$(001)_{Chl}//\{111\}_{Spl};\quad [010]_{Chl}//\langle 110\rangle_{Spl}$$

and we expect that this relationship would hold for our experimentally reacted samples. Because they have some structural similarity to chlorite, olivine and spinel will have significantly lower activation energies for nucleation than cordierite, but not as low as talc. Significantly, at 640–660 °C, olivine and spinel were found to have nucleated only on the (high energy) grain-boundaries or cleavage-planes, despite the resulting need for Al to diffuse comparatively long distances, whereas talc was able to nucleate within the chlorite because of its very much lower ΔG^*.

At 700–725 °C olivine and spinel were found along grain-boundaries and within the patches of orthopyroxene that had replaced the chlorite grains. Nucleation on less potent, intra-granular sites is to be expected at temperatures further from equilibrium, where the contribution of the driving force, ΔG_v, to the activation energy, ΔG^*, is larger.

The texture of the pyroxene in the 700–725 °C experiments suggest that the pyroxene grew from the chlorite in an oriented fashion. The structure of orthopyroxene consists of layers of oxygen ions parallel to (001) that are partially approximately close-packed, and orthopyroxene was found to form an orientated reaction product of the pyrometamorphism of chlorite with $(001)_{Chl}//(100)_{Opx}$; $[010]_{Chl}//[010]$ or $[013]_{Opx}$ (Worden *et al.*, 1987, 1988). Its structure is not, however, as close to that of chlorite as talc's, and, for that reason, orthopyroxene forms at temperatures further from equilibrium where ΔG_v is larger. The temperature range of these experiments is 50 °C or more above that of the metastable reaction that produces orthopyroxene from chlorite (the FMASH equivalent of reaction 1). Another reason for the predominance of pyrox-

ene in the 700–725 °C experiments is that, at such temperatures, talc is less stable than orthopyroxene in the presence of olivine. (In the MASH system, the assemblage MgTlc + Fo gives way to MgOpx + MgCrd at ~665 °C [Table 7]; because of the way in which Mg and Fe are partitioned between these minerals, adding iron to the system will result in minimal change in the equilibrium temperature of this reaction.) This means that at temperatures in the range 700–725 °C, formation of orthopyroxene will lower the total energy of the assemblage more than the formation of talc.

Conclusions

Natural rock samples of chlorite [Mg/(Mg + Fe) = 0.75–0.79] underwent thermal decomposition by metastable reactions 5 and 6 (above) when heated experimentally to temperatures in the range 640–725 °C at 1 kbar for 168–599 hours. The stable breakdown assemblage (Crd + Ol + Spl) was not observed in any experiment. Below 680 °C chlorite was partially replaced by talc, and olivine and spinel nucleated along chlorite/chlorite grain-boundaries. Talc nucleated in parallel orientation within the chlorite because of the close correspondence of the two structures. The ease of talc nucleation suppressed nucleation of stable cordierite. At higher temperatures (greater reaction overstepping) metastable orthopyroxene, rather than talc, replaced chlorite. Spinel and olivine nucleated both within pyroxene and along chlorite/chlorite grain-boundaries.

The mechanisms of chlorite breakdown reactions in natural rock cores under disequilibrium conditions are very different from the mechanisms observed in experiments on powdered oxides. The degree of similarity between the crystal structures of potential product phases and the reactant mineral can profoundly affect the kinetics of a decomposition reaction and may result in the nucleation of product phase well outside its stability field or inhibit the nucleation of a stable phase.

Acknowledgements

We are very grateful to Dave Plant and Tim Hopkins (Manchester University Geology Department) and Stuart Kearns and Peter Hill (Edinburgh University Geology Department) for their assistance with SEM and microprobe analyses and to Peter Kenway, Ian Brough and Graham Cliff (UMIST/Manchester University Materials Science Centre) for maintenance of the TEM facilities. We also thank Drs. Colin Graham and Steve Elphick (Edinburgh University Geology Department) for provision of experimental facilities. This work was supported by NERC Grant GR/6316 to PEC and GTRD.

References

Bell, I. A. and Wilson, C. J. L. (1977) Growth defects in metamorphic biotite. *Phys. Chem. Mineral.*, **2**, 153–69.

Brearley, A. J. (1986) An electron optical study of muscovite breakdown in pelitic xenoliths during pyrometamorphism. *Mineral. Mag.*, **50**, 385–97.

—— (1987*a*) A natural example of the disequilibrium breakdown of biotite at high temperature: TEM observations and comparison with experimental kinetic data. Ibid., **51**, 93–106.

—— (1987*b*) An experimental and kinetic study of the breakdown of aluminous biotite at 800 °C: Reaction microstructures and mineral chemistry. *Bull. Minèral.*, **110**, 512–32.

—— and Rubie, D. C. (1990) The effects of H_2O on the disequilibrium breakdown of muscovite + quartz. *J. Petrol.*, **31**, 925–56.

Brown, B. E. and Bailey, S. W. (1962) Chlorite polytypism: I. Regular and semi-random one-layer structures. *Amer. Mineral.*, **47**, 819–50.

Champness, P. E. (1970) Nucleation and growth of iron oxides in olivines, $(Mg, Fe)_2SiO_4$. *Mineral. Mag.*, **37**, 790–800.

Chernosky Jr., J. V. (1974) The upper stability of clinochlore at low pressure and the free energy of formation of Mg-cordierite. *Amer. Mineral.*, **59**, 496–507.

Cho, M. and Fawcett, J. J. (1986) A kinentic study of clinochlore and its high temperature equivalent forsterite–cordierite–spinel. Ibid., **71**, 68–77.

Droop, G. T. R. (1987) A general equation for estimating Fe^{+3} concentration in ferromagnesian silicates and oxides from microprobe analyses using stoichiometric criteria. *Mineral. Mag.*, **51**, 431–5.

Fawcett, J. J. and Yoder, H. S. (1966) Phase relationships of chlorite in the system $MgO–Al_2O_3–SiO_2–H_2O$. *Amer. Mineral.*, **51**, 353–87.

Fleming, P. D. and Fawcett, J. J. (1976) Upper stability of chlorite + quartz in the system $MgO–FeO–Al_2O_3–SiO_2–H_2O$ at 2 kbar water pressure. Ibid., **61**, 1175–93.

Herzberg, C. T. (1983) The reaction forsterite + cordierite = aluminous orthopyroxene + spinel in the system $MgO–Al_2O_3–SiO_2$. *Contrib. Mineral. Petrol.*, **84**, 84–90.

Holland, T. J. B. and Powell, R. (1990) An enlarged and updated internally consistent thermodynamic dataset with uncertainties and correlations: the system $K_2O–Na_2O–CaO–MgO–MnO–FeO–Fe_2O_3–Al_2O_3–TiO_2–SiO_2–C–H_2–O_2$. *J. Metamorphic Geol.*, **8**, 89–124.

Jenkins, D. M. and Chernosky Jr., J. V. (1986) Phase equilibria and crystallochemical properties of Mg-chlorite. *Amer. Mineral.*, **71**, 924–36.

Kretz, R. (1983) Symbols for rock-forming minerals. Ibid., **68**, 277–9.

McOnie, A. W., Fawcett, J. J., Jeffrey, J., and James, R. S. (1975) The stability of intermediate chlorites of

the clinochlore-daphnite series at 2 kbar P_{H_2O}. Ibid., **60**, 1047–62.

Nelson, B. W. and Roy, R. (1958) Synthesis of the chlorites and their structural and chemical constitution. Ibid., **43**, 707–25.

Powell, R. and Holland, T. J. B. (1988) An internally consistent dataset with uncertainties and correlations: 3. Application to geobarometry, worked examples and a computer program. *J. Metamorphic Geol.*, **6**, 173–204.

Robie, R. A., Hemingway, B. S., and Fisher, J. R. (1978) Thermodynamic properties of minerals and related substances at 298.15 K and 1 bar (10^5 pascals) pressure and at higher temperatures. *United States Geol. Survey Bulletin*, **1452**.

Roy, D. M. and Roy, R. (1955) Synthesis and stability of minerals in the system $MgO–Al_2O_3–SiO_2–H_2O$. *Amer. Mineral.*, **40**, 147–78.

Rubie, D. C. and Brearley, A. J. (1987) Metastable melting during the breakdown of muscovite + quartz at 1 kbar. *Bull. Minéral.*, **110**, 533–49.

—— —— (1991 submitted) Kinetics of partial melting of muscovite + quartz and rates of multicomponent diffusion in H_2O-saturated granitic liquid. *Geochim. Cosmochim. Acta*.

Seifert, F. (1974) Stability of sapphirine: a study of the aluminous part of the system $MgO–Al_2O_3–SiO_2–H_2O$. *J. Geol.*, **82**, 173–204.

Velde, B. (1973) Phase equilibria in the system $MgO–Al_2O_3–SiO_2–H_2O$: chlorites and associated minerals. *Mineral Mag.*, **39**, 297–312.

Wirth, R. (1986) Thermal alteration of glaucophane in the contact aureole of the Traversella Intrusion (N. Italy). *Neus. Jahrb. Min. Abh.*, **154**, 193–205.

Wood, B. J. and Banno, S. (1973) Garnet–orthopyroxene and orthopyroxene–clinopyroxene relationships in simple and complex systems. *Contrib. Mineral. Petrol.*, **42**, 109–24.

Worden, R. H., Champness, P. E. and Droop, G. T. R. (1987) Transmission electron microscopy of pyrometamorphic breakdown of phengite and chlorite. *Mineral. Mag.*, **51**, 107–21.

—— —— —— (1988) Mechanisms of thermal decomposition of sheet silicates in rocks. *Proc. Intl. Conf. on Phase Transformation*, Cambridge, 1987, Inst. Metals, 614–17.

—— Droop, G. T. R. and Champness, P. E. (1992) The influence of crystallography and kinetics on phengite breakdown reactions in a low-pressure metamorphic aureole. *Contrib. Mineral. Petrol.*, **110**, 329–45.

[*Manuscript received 5 September 1991: revised 5 August 1992*]

Appendix

Abbreviations for mineral names and end-member components (asterisked). Adapted from Kretz (1983).

*Ames	Amesite
Chl	Chlorite
*Chr	Chrysotile
*Clin	Clinochlore
Crd	Cordierite
*Crn	Corundum
*En	Enstatite
*Fo	Forsterite
MgAth	Aluminous Mg Orthoamphibole solid solution
MgChl	Aluminous Mg Chlorite solid solution
*MgCrd	MgCordierite
MgOpx	Aluminous Mg orthopyroxene solid solution
*MgSpl	MgSpinel
*MgTa	Al-free Mg Talc
MgTlc	Aluminous Mg Talc solid solution
*MgTs	MgTschermaks Pyroxene
Ol	Olivine
Opx	Orthopyroxene
*Qtz	β-Quartz
Spl	Spinel
*TaTs	MgTschermaks Talc
Tlc	Talc